EUROPEAN JOURNAL OF PURE AND APPLIED MATHEMATICS
2025, Vol. 18, Issue 3, Article Number 6347
ISSN 1307-5543 – ejpam.com
Published by New York Business Global

Mathematical Modeling of SARS-CoV-2 Epidemics Using Fractional Calculus and Optimal Interventions

Nadeem Abbas[1], Wasfi Shatanawi[1,2,*], Syeda Alishwa Zanib[3]

[1] *Department of Mathematics and Sciences, College of Humanities and Sciences, Prince Sultan University, Riyadh, 11586, Saudi Arabia*
[2] *Department of Mathematics, Faculty of Science, The Hashemite University, P.O Box 330127, Zarqa 13133, Jordan*
[3] *Department of Mathematics, Riphah International University, Main Satyana Road, Faisalabad 44000, Pakistan*

Abstract. In December 2019, the SARS-CoV-2 (COVID-19) virus was identified and quickly spread worldwide, causing a major global health crisis. To investigate its transmission dynamics, we developed a ten-compartment mathematical model, named CoVCom10, which includes key stages such as asymptomatic (F), pre-symptomatic (E), and vaccinated (V) individuals. The basic reproduction number (R_0) has been calculated to evaluate how easily the virus can spread. We analyzed the local and global stability of the disease-free equilibrium and prove that the disease under control after vaccination when $R_0 < 1$. A sensitivity analysis was conducted to assess the impact of key parameters, including the vaccination rate from susceptible individuals (β), transmission from susceptible to pre-symptomatic individuals (ϕ), and the rate of vaccination from pre-symptomatic individuals (γ). To evaluate intervention strategies, we extended the model by incorporating time-dependent control variables representing vaccination (a_1), hospitalization (a_2), and isolation of asymptomatic individuals (a_3). The Pontryagin Maximum Principle was applied to identify optimal control strategies. Numerical simulations reveal that these interventions significantly reduce virus transmission, particularly as the fractional-order parameter (ς) approaches 1, which aligns with observed real-world disease dynamics. The study emphasizes the effectiveness of integrated vaccination and treatment strategies in controlling the spread of COVID-19.

2020 Mathematics Subject Classifications: 26A33, 34A08, 03C65

Key Words and Phrases: SARS-CoV-2, Fractional-Order Model, Compartmental Model, Basic Reproduction Number, Stability Analysis, Pontryagin's Maximum Principle

*Corresponding author.
DOI: https://doi.org/10.29020/nybg.ejpam.v18i3.6347

Email addresses: nabbas@psu.edu.sa (N. Abbas), wshatanawi@psu.edu.sa (W. Shatanawi), 19907@riphahfsd.edu.pk (S. A. Zanib)

1. Introduction

In the middle of the 1960s, human coronaviruses were first discovered. The well-known coronaviruses that may infect individuals include SARS-CoV (severe acute respiratory syndrome), MERS-CoV (Middle East Respiratory Syndrome), and SARS-CoV-2 (the new coronavirus that causes coronavirus disease 2019, or COVID-19), which is the subject of this research. Corona, virus, and disease are represented, respectively, by the letters CO, VI, and D in COVID-19. In December 2019, a novel virus was discovered during an outbreak in Wuhan, China [1–4] shown in Figure 1. There were attempts to control it, but they did not succeed, allowing the virus to spread to other regions of China and, subsequently the propagation of the world. According to a survey of individuals who passed away, the majority of them were elderly or had serious diseases like parkinson's, lung, diabetes, chronic heart, or kidney disease. Flu and other viruses that can propagate contact with the mouth and touch with the nose can spread quickly. Coronaviruses are very dangerous and spread readily from person to person [5].

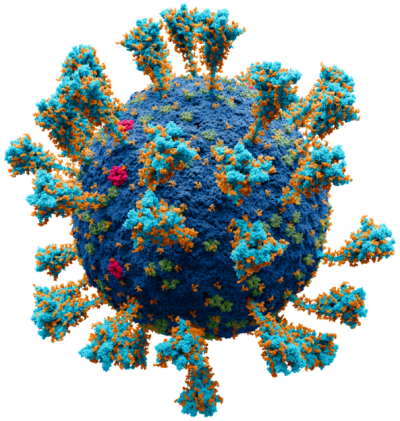

Figure 1: *SARS-CoV-2 Structure*

Many mathematicians are constantly working to construct new, more effective models that may be used for modeling to evaluate the relationship between death and infection, fluid dynamic and predict how it will spread in the future [6–9]. Fractional calculus plays a vital role in biological modeling, offering a more accurate and flexible framework for capturing the memory and hereditary characteristics inherent in biological systems. Numerous researchers have developed mathematical models using fractional calculus to enhance the precision of numerical simulations and better reflect real-world disease dynamics [10]. In a short period, various types of research on COVID-19 model, pandemic have been conducted in the literature. Diagne et al., (2021) [11] studied formulation of COVID-19 model with vaccination. In their model, Various epidemiological stages were created for the entire population N based on each person's health at any given moment t. They was shown how to regulate the model to minimize the spread of COVID-19 by employing Pontryagin's maximal principle. Acheampong et al., (2022) [12] developed a model where

Pre-Symptomatic and infectious epidemiological classes generate infectious disease models, leaving them as abstract ideas. Because of the prevalence of asymptomatic carriers, it was difficult to identify those who have been Pre-Symptomatic (represented by E) to or infected (represented by I) with SARS-CoV-2. They had produced two epidemiological classes: (1) a known group of Pre-Symptomatic individuals thought to be SARS-CoV-2 (represented by Q), and (2) those whose SARS-CoV-2 status has been clinically verified (represented by P). Those who have been recognized as vulnerable were marked with the letter Q as they were required to quarantine under Ghana's COVID-19 principles. The same was applied to confirm positive (P) where clinical tests have shown that they had SARS-CoV-2. They named their model CoVCom-9. Butt et al. (2023) [13] developed a nonlinear SEIQHR fractional model for COVID-19 using the Atangana–Baleanu (ABC) derivative to capture the complex dynamics of disease transmission. They analyzed equilibrium points, performed sensitivity and bifurcation analyses, and applied an optimal control framework with the Toufik–Atangana numerical method to assess control strategies. Zanib et al., (2024) [14] developed a modified compartmental COVID-19 model incorporating vaccination strategies using conformable fractional derivatives to capture complex transmission dynamics. The basic reproduction number R_0, its sensitivity indices, and the model's stability were analyzed, with a finite difference method providing accurate numerical solutions and highlighting the role of vaccination in disease control. Butt et al., (2024) [15] developed a nonlinear fractional bi-susceptible $S_1S_2V_1V_2IHR$ model using the Atangana–Baleanu Caputo derivative to investigate the dynamics and control of COVID-19. They analyzed the model's stability, validated results using the Toufik–Atangana numerical method, and demonstrated the effectiveness of optimized control strategies through simulations. Abboubakar and Racke (2025) [16] developed a COVID-19 model using integer and Caputo fractional-order derivatives, incorporating vaccination, confinement, and treatment with limited resources. Using German data, it was shown that the fractional model provided more accurate long-term forecasts, with a reproduction number around 1.90, indicating endemic persistence. Kumar et al., (2025)[17] developed an age-structured SEIR model to analyze the spread of COVID-19 and estimate key parameters such as the basic reproduction number R_0 and case fatality ratio (CFR). The model, validated using epidemiological data and uncertainty analysis, provided insights for public health interventions and was suggested to be extended using agent-based modeling. While reviewing the literature, we observed that many existing COVID-19 models skip critical components, particularly the inclusion of a vaccinated compartment. This limitation reduces their capacity to realistically capture disease dynamics in the post-vaccine era. To address this gap, we developed a comprehensive model that consist for all possible stages of COVID-19 progression. Specifically, we propose a ten-compartment mathematical model, termed CoVCom10, which incorporates key categories such as asymptomatic (F), pre-symptomatic (E), and vaccinated (V) individuals. CoVCom10 builds upon the previous CoVCom9 framework by incorporating the vaccination compartment, enabling a more accurate simulation of immunization effects on SARS-CoV-2 transmission. The addition of asymptomatic and pre-symptomatic compartments is essential for capturing hidden transmission routes and reflecting the full spectrum of COVID-19 progression. These

improvements enhance the epidemiological relevance of the model and support the evaluation of various intervention strategies. To further improve the model's realism, we employ the conformable fractional derivative, which accounts for memory and hereditary effects. This approach enables the model to incorporate the influence of past states on current dynamics, thereby capturing complex behaviors such as delayed responses and long-term persistence of infections. The conformable fractional framework preserves key properties of classical calculus while offering improved computational tractability compared to other fractional definitions. Notably, it reduces to the classical model when the fractional order approaches one, ensuring consistency with traditional differential models. To validate the model's applicability, we compared its simulation results with real-world COVID-19 data [18]. This comparison confirms the model's capability to realistically represent the pandemic's progression and evaluate the effectiveness of various public health measures. Despite the computational challenges associated with solving fractional differential equations, the proposed model offers a valuable and flexible framework for analyzing the roles of vaccination, asymptomatic carriers, and control strategies in managing COVID-19 outbreaks.

2. Model Description and Formulation

Table 1: *List of Symbols, Parameters, and Abbreviations*

State Variables	
$S(t)$	Number of susceptible individuals at time t
$E(t)$	Number of pre-symptomatic individuals at time t
$U(t)$	Number of infected individuals at time t
$Q(t)$	Number of quarantined individuals at time t
$P(t)$	Number of confirmed positive individuals at time t
$H(t)$	Number of hospitalized individuals in ordinary wards at time t
$C(t)$	Number of individuals in intensive care unit at time t
$F(t)$	Number of asymptomatic individuals at time t
$V(t)$	Number of vaccinated individuals at time t
$R(t)$	Number of recovered individuals at time t
Model Parameters	
ϕ	Transmission rate from S to E
λ_1	Transition rate from E to U
λ_2	Transition rate from E to Q
γ	Transition rate from E to V
α_1	Recovery rate of U
α_2	Transition rate from U to P
b_1	Transition rate from Q to S
b_2	Transition rate from Q to V
b_3	Transition rate from Q to P
φ_1	Transition rate from P to H
φ_2	Transition rate from P to C
φ_3	Transition rate from P to F
m_1	Recovery rate from H
m_2	Transition rate from H to C
m_3	Transition rate from H to F
σ_1	Self-isolation rate of F
σ_2	Transition rate from F to H
η	Recovery rate from C to H
β	Vaccination rate of S
Λ	Recruitment/birth rate into S
μ	Natural death rate
d_1–d_7	Disease-induced death rates in E, U, Q, P, H, C, and F
τ	Loss of immunity rate from R to S
Abbreviations	
DFEP	Disease-Free Equilibrium Point
SARS-CoV-2	Severe Acute Respiratory Syndrome Coronavirus 2
COVID-19	Coronavirus Disease 2019
CoVCom10	Coronavirus Compartment Model with 10 compartments
CFD	Conformable Fractional Derivative

The total population $\mathbb{N}(t)$ is stratified into ten distinct epidemiological compartments to comprehensively capture the transmission dynamics of COVID-19, as illustrated in the flowchart in Figure 2. The transitions between these compartments occur in continuous time and are governed by a system of nonlinear ordinary differential equations.

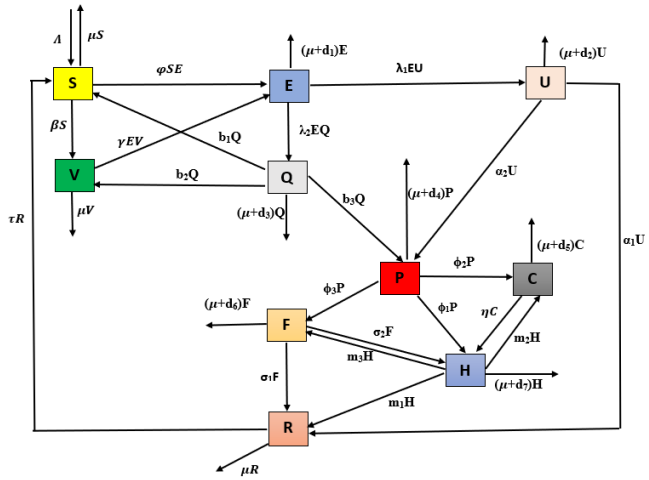

Figure 2: *Schematic diagram of the CoVCom10 compartmental model.*

The governing system for the model is system of differential equations shown below:

$$
\begin{aligned}
\frac{dS}{dt} &= \Lambda + \tau R + b_2 Q - (\phi E + \beta + \mu)\, S,\\
\frac{dE}{dt} &= \phi\, ES + \gamma\, VE - (\lambda_1 U + \lambda_2 Q + \mu + d_1)\, E,\\
\frac{dU}{dt} &= \lambda_1 EU - (\alpha_1 + \alpha_2 + \mu + d_2)\, U,\\
\frac{dQ}{dt} &= \lambda_2 EQ - (b_1 + b_2 + b_3 + \mu + d_3)\, Q,\\
\frac{dP}{dt} &= \alpha_2 U + b_1 Q - (\varphi_1 + \varphi_2 + \varphi_3 + \mu + d_4)\, P,\\
\frac{dH}{dt} &= \varphi_1 P + \eta\, C + \sigma_2 F - (m_1 + m_2 + m_3 + \mu + d_5)\, H,\\
\frac{dC}{dt} &= \varphi_2 P + m_2 H - (\eta + \mu + d_6)\, C,\\
\frac{dF}{dt} &= \varphi_3 P + m_3 H - (\sigma_1 + \sigma_2 + \mu + d_7)\, F,\\
\frac{dV}{dt} &= \beta\, S + b_3 Q - (\gamma\, E + \mu)\, V,\\
\frac{dR}{dt} &= \sigma_1 F + \alpha_1 U + m_1 H - (\tau + \mu)\, R.
\end{aligned}
\tag{2.1}
$$

Therefore,

$$\mathbb{N}(t) = S(t) + E(t) + U(t) + Q(t) + P(t) + H(t) + C(t) + F(t) + V(t) + R(t).$$

Each compartment, along with its associated abbreviation and biological interpretation, is detailed in Table 1, which also includes a complete list of model parameters and their descriptions.

Fractional-Order Model Formulation

Khalil et al. [19] introduced the conformable fractional derivative (CFD), a mathematical operator that generalizes classical calculus while maintaining key differential properties. The CFD of order $\zeta \in (0, 1]$ is defined as:

$$D_t^{\zeta} M(t) = \lim_{\epsilon \to 0} \frac{M(t + \epsilon t^{1-\zeta}) - M(t)}{\epsilon}, \tag{2.2}$$

which simplifies to the classical derivative when $\zeta = 1$. This operator satisfies the composition rule:

$$D_t^{\zeta} M(t) = t^{1-\zeta} \frac{dM}{dt}. \tag{2.3}$$

To capture memory effects in COVID-19 transmission, we reformulate the CoVCom10 model (2.1) using the CFD framework [19]:

$$\begin{aligned}
D_t^{\zeta} S &= \Lambda + \tau R + b_2 Q - (\phi E + \beta + \mu) S, \\
D_t^{\zeta} E &= \phi E S + \gamma V E - (\lambda_1 U + \lambda_2 Q + \mu + d_1) E, \\
D_t^{\zeta} U &= \lambda_1 E U - (\alpha_1 + \alpha_2 + \mu + d_2) U, \\
D_t^{\zeta} Q &= \lambda_2 E Q - (b_1 + b_2 + b_3 + \mu + d_3) Q, \\
D_t^{\zeta} P &= \alpha_2 U + b_1 Q - (\varphi_1 + \varphi_2 + \varphi_3 + \mu + d_4) P, \\
D_t^{\zeta} H &= \varphi_1 P + \eta C + \sigma_2 F - (m_1 + m_2 + m_3 + \mu + d_5) H, \\
D_t^{\zeta} C &= \varphi_2 P + m_2 H - (\eta + \mu + d_6) C, \\
D_t^{\zeta} F &= \varphi_3 P + m_3 H - (\sigma_1 + \sigma_2 + \mu + d_7) F, \\
D_t^{\zeta} V &= \beta S + b_3 Q - (\gamma E + \mu) V, \\
D_t^{\zeta} R &= \sigma_1 F + \alpha_1 U + m_1 H - (\tau + \mu) R.
\end{aligned} \tag{2.4}$$

The system is solved under non-negative initial conditions:

$$\begin{aligned}
&S(0) = S_0 \geq 0, \quad E(0) = E_0 \geq 0, \quad U(0) = U_0 \geq 0, \\
&Q(0) = Q_0 \geq 0, \quad P(0) = P_0 \geq 0, \quad H(0) = H_0 \geq 0, \\
&C(0) = C_0 \geq 0, \quad F(0) = F_0 \geq 0, \quad V(0) = V_0 \geq 0, \\
&R(0) = R_0 \geq 0.
\end{aligned} \tag{2.5}$$

Mathematical Analysis

The biologically feasible region for the fractional-order model (2.4) is defined as:

$$\mathcal{D} = \Bigg\{(S(t), E(t), U(t), Q(t), P(t), H(t), C(t), F(t), V(t), R(t)) \in \mathbb{R}_+^{10} : \\ S + E + U + Q + P + H + C + F + V + R \leq \frac{\Lambda}{\mu}\Bigg\}, \tag{2.6}$$

where $\mathcal{D}$ forms a positive invariant set that captures all epidemiologically meaningful states of the system. The mathematical analysis of the model demonstrate the the feasible region $\mathcal{D}$ in terms of bounded and non-negative, stability results, and epidemiological thresholds. Solutions of equations (2.4) with initial conditions (2.5) keep in $\mathcal{D}$ discuss in the below theorem.

Theorem 1. ***(Positive Invariance of Feasible Region)*** *For the fractional-order system (2.4) with non-negative initial conditions (2.5), the closed set $\mathcal{D}$ defined in (2.6) forms a positively invariant region under conformable fractional dynamics when all parameters satisfy $\{\phi, \beta, \mu, \ldots\} \in \mathbb{R}_+$.*

Proof. Let $\mathbb{N}(t) = \sum_{i=1}^{10} X_i(t)$ represent the total population, where X_i denotes each compartment. Applying the conformable fractional derivative operator:

$$D_t^{\zeta}\mathbb{N}(t) = \Lambda - \mu\mathbb{N}(t) - \sum_{i=1}^{7} d_i X_i(t). \tag{2.7}$$

Using the conformable derivative property $D_t^{\zeta}\mathbb{N} = t^{1-\zeta}\frac{d\mathbb{N}}{dt}$, we rewrite:

$$t^{1-\zeta}\frac{d\mathbb{N}}{dt} = \Lambda - \mu\mathbb{N} - \underbrace{\sum_{i=1}^{7} d_i X_i(t)}_{\geq 0}. \tag{2.8}$$

This establishes the inequality:

$$\frac{d\mathbb{N}}{dt} \leq t^{\zeta-1}(\Lambda - \mu\mathbb{N}). \tag{2.9}$$

Solving this fractional differential inequality through separation of variables:

$$\int_{\mathbb{N}(0)}^{\mathbb{N}(t)} \frac{d\mathbb{N}}{\Lambda - \mu\mathbb{N}} \leq \int_0^t \tau^{\zeta-1} d\tau, \tag{2.10}$$

taking integrated factor and after simplify:

$$\mathbb{N}(t) \leq \frac{\Lambda}{\mu} - \left(\frac{\Lambda}{\mu} - \mathbb{N}(0)\right)\exp\left(-\frac{\mu}{\zeta}t^{\zeta}\right). \tag{2.11}$$

For $\mathbb{N}(0) \leq \frac{\Lambda}{\mu}$, the exponential term ensures $\mathbb{N}(t) \leq \frac{\Lambda}{\mu}\ \forall t \geq 0$. Thus, all solutions remain bounded within $\mathcal{D}$, making it positively invariant under the fractional-order dynamics.

Positivity and Boundedness of Solutions

Theorem 2. *For the fractional-order system (2.4) with non-negative initial conditions (2.5) and non-negative parameters, the following holds:*

- *All solutions* $\{S(t), E(t), U(t), Q(t), P(t), H(t), C(t), F(t), V(t), R(t)\}$ *remain non-negative for all* $t \geq 0$.
- *The total population satisfies* $\limsup_{t\to\infty} \mathbb{N}(t) \leq \frac{\Lambda}{\mu}$.

Proof. **Positivity**
Consider the conformable fractional derivative formulation $D_t^{\zeta} X = t^{1-\zeta} X'$. For each compartment $X \in \{S, E, U, Q, P, H, C, F, V, R\}$:

Lemma 1. *Let* $D_t^{\zeta} X \geq -\psi X$ *with* $\psi \geq 0$ *and* $X(0) \geq 0$. *Then* $X(t) \geq 0\ \forall t \geq 0$.

For the susceptible population:

$$D_t^{\zeta} S = \Lambda + \tau R + b_2 Q - (\phi E + \beta + \mu) S \geq -(\phi E + \beta + \mu) S, \tag{2.12}$$

Applying the comparison principle for fractional differential equations:

$$S(t) \geq S(0) \exp\left(-\frac{1}{\zeta}(\phi E + \beta + \mu) t^{\zeta}\right) \geq 0. \tag{2.13}$$

Similar analysis for other compartments yields:

$$\begin{aligned} D_t^{\zeta} E &\geq -(\lambda_1 U + \lambda_2 Q + \mu + d_1) E, \\ D_t^{\zeta} U &\geq -(\alpha_1 + \alpha_2 + \mu + d_2) U, \\ &\vdots \end{aligned} \tag{2.14}$$

By sequential application of the comparison lemma, all compartments maintain non-negativity.

Boundedness
From Theorem 1 (Positive Invariance of Feasible Region), the total population dynamics satisfy:

$$D_t^{\zeta} \mathbb{N} = \Lambda - \mu \mathbb{N} - \sum_{i=1}^{7} d_i X_i \leq \Lambda - \mu \mathbb{N}. \tag{2.15}$$

Solving the fractional inequality:

$$\mathbb{N}(t) \leq \frac{\Lambda}{\mu} - \left(\frac{\Lambda}{\mu} - \mathbb{N}(0)\right) \exp\left(-\frac{\mu}{\zeta} t^{\zeta}\right). \tag{2.16}$$

As $t \to \infty$, the exponential term vanishes, yielding:

$$\limsup_{t\to\infty} \mathbb{N}(t) \leq \frac{\Lambda}{\mu}. \tag{2.17}$$

2.1. Disease-free Equilibrium Point

The disease-free equilibrium point (DFE) [20] of the model is determined by setting all compartments associated with infection to zero, reflecting the absence of disease in the population. Specifically, we set

$$E = U = Q = P = H = C = F = R = 0.$$

At equilibrium, the rates of change for the susceptible (S) and vaccinated (V) compartments are given by the following steady-state equations:

$$\frac{dS}{dt} = \Lambda - (\beta + \mu)S = 0,$$
$$\frac{dV}{dt} = \beta S - \mu V = 0.$$

Solving these equations yields the equilibrium values:

$$S^* = \frac{\Lambda}{\beta + \mu}, \quad V^* = \frac{\Lambda\beta}{(\beta + \mu)\mu}. \tag{2.18}$$

Therefore, the disease-free equilibrium point is

$$E_0 = (S, E, U, Q, P, H, C, F, V, R) = \left(\frac{\Lambda}{\beta + \mu}, 0, 0, 0, 0, 0, 0, 0, \frac{\Lambda\beta}{(\beta + \mu)\mu}, 0\right).$$

3. Basic Reproduction Number

To analyze the transmission potential of the CoVCom10 model (2.4), we employ the next-generation matrix approach developed by Van den Driessche and Watmough [21]. This method involves decomposing the system into two main components: the transmission matrix, which describes the generation of new infections, and the transition matrix, which captures the movement of individuals between different epidemiological states.

The transmission matrix $\mathbb{A}(x^*)$ and the transition matrix $\mathbb{B}(x^*)$ are constructed as follows:

$$\mathbb{A}(x^*) = \begin{bmatrix} \gamma VE + \phi ES \\ \lambda_1 EU \\ \lambda_2 EQ \\ 0 \\ 0 \\ 0 \\ 0 \end{bmatrix}, \tag{3.19}$$

$$\mathbb{B}(x^*) = \begin{bmatrix} -\Pi_1 E \\ -\Pi_2 U \\ -\Pi_3 Q \\ \alpha_2 U + b_1 Q - \Pi_4 P \\ \eta\, C + \sigma_2 F - \Pi_5 H + \varphi_1 P \\ -\Pi_6 C + m_2 H + \varphi_2 P \\ -\Pi_7 F + m_3 H + \varphi_3 P \end{bmatrix}. \tag{3.20}$$

The next-generation matrix $\mathbb{A}\mathbb{B}^{-1}$ evaluated at the disease-free equilibrium yields,

$$\mathbb{A}\mathbb{B}^{-1} = \begin{bmatrix} \frac{1}{\Pi_1}\left(\frac{\phi\,\Lambda}{\beta+\mu} + \frac{\beta\,\Lambda\,\gamma}{(\beta+\mu)\mu}\right) & 0 & 0 & 0 & 0 & 0 & 0 \\ 0 & 0 & 0 & 0 & 0 & 0 & 0 \\ 0 & 0 & 0 & 0 & 0 & 0 & 0 \\ 0 & 0 & 0 & 0 & 0 & 0 & 0 \\ 0 & 0 & 0 & 0 & 0 & 0 & 0 \\ 0 & 0 & 0 & 0 & 0 & 0 & 0 \\ 0 & 0 & 0 & 0 & 0 & 0 & 0 \end{bmatrix}. \tag{3.21}$$

Here, the composite parameters Π_i are defined to combine various transition rates:

$$\begin{aligned} \Pi_1 &= \lambda_1 U + \lambda_2 Q + \mu + d_1, \\ \Pi_2 &= \alpha_1 + \alpha_2 + \mu + d_2, \\ \Pi_3 &= b_1 + b_2 + b_3 + \mu + d_3, \\ \Pi_4 &= \varphi_1 + \varphi_2 + \varphi_3 + \mu + d_4, \\ \Pi_5 &= m_1 + m_2 + m_3 + \mu + d_5, \\ \Pi_6 &= \eta + \mu + d_6, \\ \Pi_7 &= \sigma_1 + \sigma_2 + \mu + d_7. \end{aligned} \tag{3.22}$$

By evaluating the Jacobians of $\mathbb{A}(x^*)$ and $\mathbb{B}(x^*)$ at the disease-free equilibrium (DFE) and computing the spectral radius of $\mathbb{A}\mathbb{B}^{-1}$, we obtain the basic reproduction number:

$$R_0 = \frac{\Lambda\ (\gamma\,\beta + \mu\,\phi)}{\mu\ (\beta+\mu)\,(\mu+d_1)}. \tag{3.23}$$

3.1. Sensitivity Analysis

Sensitivity analysis quantifies how variations in model parameters affect the basic reproduction number R_0 [22]. The normalized sensitivity index, defined as $\Upsilon_{\xi}^{R_0}$, represents

the relative change in R_0 resulting from a relative change in a parameter ξ, mathematically given by:

$$\Upsilon_{\xi}^{R_0} = \frac{\partial R_0}{\partial \xi} \times \frac{\xi}{R_0}. \tag{3.24}$$

Applying this definition to model reproduction number:

$$R_0 = \frac{\Lambda\,(\gamma\,\beta + \mu\,\phi)}{\mu\,(\beta + \mu)\,(\mu + d_1)}, \tag{3.25}$$

we compute sensitivity indices for key parameters:

- **Sensitivity with respect to** β:

$$\Upsilon_{\beta}^{R_0} = \frac{\gamma\,\beta}{\gamma\,\beta + \mu\,\phi} - \frac{\beta}{\beta + \mu}. \tag{3.26}$$

  An increase in β will increase R_0, indicating a higher transmission potential.

- **Sensitivity with respect to** γ:

$$\Upsilon_{\gamma}^{R_0} = \frac{\gamma\,\beta}{\gamma\,\beta + \mu\,\phi}. \tag{3.27}$$

  A higher γ elevates R_0, highlighting increased transmission from asymptomatic or pre-symptomatic individuals.

- **Sensitivity with respect to** ϕ:

$$\Upsilon_{\phi}^{R_0} = \frac{\mu\,\phi}{\gamma\,\beta + \mu\,\phi}. \tag{3.28}$$

  An increase in exposure rate ϕ raises R_0, demonstrating greater susceptibility within the population.

- **Sensitivity with respect to** μ:

$$\Upsilon_{\mu}^{R_0} = \frac{\mu\,\phi}{\gamma\,\beta + \mu\,\phi} - \frac{\mu}{\beta + \mu} - \frac{\mu}{\mu + d_1} - 1. \tag{3.29}$$

  Increasing the natural death rate μ generally reduces R_0, as fewer individuals remain susceptible to infection.

- **Sensitivity with respect to** d_1:

$$\Upsilon_{d_1}^{R_0} = -\frac{d_1}{\mu + d_1}. \tag{3.30}$$

  Increasing disease-induced death rate d_1 lowers R_0, due to a reduction in the number of infectious contacts.

- **Sensitivity with respect to** Λ:

$$\Upsilon_{\Lambda}^{R_0} = 1. \tag{3.31}$$

An increase in Λ which is birth rate will increase R_0, indicating a higher transmission potential.

This sensitivity analysis identifies critical parameters influencing disease dynamics, guiding effective strategies for controlling the epidemic shown in Figure 3.

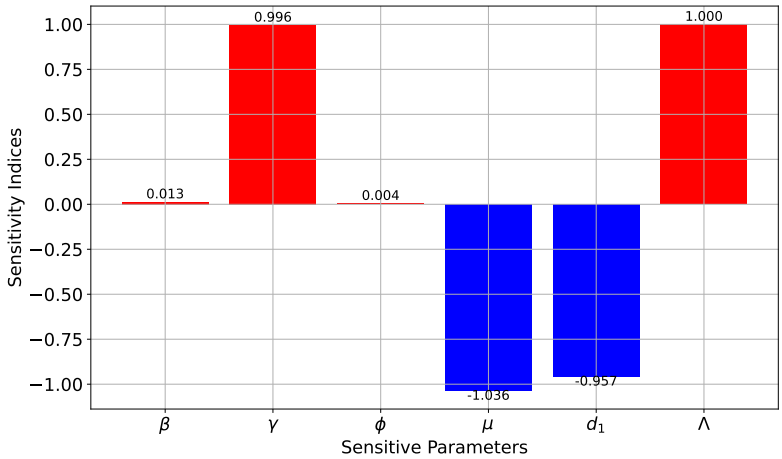

Figure 3: *Sensitivity analysis*

3.2. Stability Analysis

Local Stability of Disease-Free Equilibrium Point

To assess the behavior of the CoVCom10 model (2.4) near the disease-free equilibrium, it is essential to analyze its local stability. This analysis determines whether small disturbances from the disease-free state will decay or grow, which is crucial for understanding epidemic control strategies. The following theorem and proof outline the conditions under which the disease-free equilibrium point (DFEP) is locally asymptotically stable.

Theorem 3. *The disease-free equilibrium point E_0 of the CoVCom10 model (2.4) is locally asymptotically stable if the basic reproduction number $R_0 < 1$ and unstable if $R_0 > 1$ [23].*

Proof. To establish the local stability of the DFEP, we compute the Jacobian matrix of the system at E_0. The Jacobian matrix J_0 is given by:

$$J_0 = \begin{bmatrix} -\beta-\mu & -\frac{\phi\Lambda}{\beta+\mu} & 0 & b_2 & 0 & 0 & 0 & 0 & 0 & \tau \\ 0 & \frac{\gamma\beta\Lambda}{(\beta+\mu)\mu}+\frac{\phi\Lambda}{\beta+\mu}-\Pi_1 & 0 & 0 & 0 & 0 & 0 & 0 & 0 & 0 \\ 0 & 0 & -\Pi_2 & 0 & 0 & 0 & 0 & 0 & 0 & 0 \\ 0 & 0 & 0 & -\Pi_3 & 0 & 0 & 0 & 0 & 0 & 0 \\ 0 & 0 & \alpha_2 & b_1 & -\Pi_4 & 0 & 0 & 0 & 0 & 0 \\ 0 & 0 & 0 & 0 & \varphi_1 & -\Pi_5 & \eta & \sigma_2 & 0 & 0 \\ 0 & 0 & 0 & 0 & \varphi_2 & m_2 & -\Pi_6 & 0 & 0 & 0 \\ 0 & 0 & 0 & 0 & \varphi_3 & m_3 & 0 & -\Pi_7 & 0 & 0 \\ \beta & -\frac{\gamma\beta\Lambda}{(\beta+\mu)\mu} & 0 & b_3 & 0 & 0 & 0 & 0 & -\mu & 0 \\ 0 & 0 & \alpha_1 & 0 & 0 & m_1 & 0 & \sigma_1 & 0 & -\tau-\mu \end{bmatrix} \tag{3.32}$$

The characteristic equation of J_0 is obtained from $\det(J_0 - \Delta\mathbb{I}) = 0$, where $\mathbb{I}$ is the identity matrix. The coefficients of the characteristic polynomial are:

$$\begin{aligned} c_1 &= 1, \\ c_2 &= \Pi_5 + \Pi_6 + \Pi_7, \\ c_3 &= (\Pi_5 + \Pi_7)\Pi_6 - \eta m_2 - m_3\sigma_2 + \Pi_5\Pi_7, \\ c_4 &= (\Pi_5\Pi_7 - m_3\sigma_2)\Pi_6 - \eta\Pi_7 m_2. \end{aligned} \tag{3.33}$$

The characteristic polynomial can be written as:

$$\begin{aligned} \frac{1}{\mu(\beta+\mu)} \big[&(\beta+\mu+\Delta)(\Delta\mu\beta + \Delta\mu^2 - \Lambda\beta\gamma - \Lambda\mu\phi + \beta\mu\Pi_1 + \mu^2\Pi_1) \\ &\times (\Pi_2+\Delta)(\Pi_3+\Delta)^2(\Pi_4+\Delta)(\mu+\Delta)(\tau+\mu+\Delta)^2 \\ &\times(\beta+\mu+\Delta)(c_1\Delta^3 + c_2\Delta^2 + c_3\Delta + c_4)\big] = 0 \end{aligned} \tag{3.34}$$

The first seven roots of the characteristic equation are:

$$\begin{aligned} \Delta_1 &= -(\beta+\mu), \\ \Delta_2 &= (R_0 - 1)\left(\frac{1}{\mu(\beta+\mu)}\right), \\ \Delta_3 &= -\Pi_4, \\ \Delta_4 &= -\mu, \\ \Delta_5 &= -(\tau+\mu), \\ \Delta_6 &= -\Pi_3, \\ \Delta_7 &= -(\tau+\mu). \end{aligned} \tag{3.35}$$

All explicit eigenvalues have negative real parts when $R_0 < 1$. For the cubic polynomial $c_1\Delta^3 + c_2\Delta^2 + c_3\Delta + c_4 = 0$, the Routh-Hurwitz stability conditions are:

$$c_1 > 0, \quad c_2 > 0, \quad c_1c_2c_3 > c_3^2 + c_1^2c_4. \tag{3.36}$$

These conditions are satisfied when $R_0 < 1$, as confirmed by the structure of the composite parameters Π_i. Therefore, all eigenvalues of the Jacobian matrix J_0 have negative real parts if and only if $R_0 < 1$, ensuring local asymptotic stability of the DFEP. Conversely, if $R_0 > 1$, the DFEP becomes unstable, indicating the potential for an epidemic outbreak.

Global Stability of Disease-Free Equilibrium Point

Lemma 2. *(Castillo-Chavez Method [24]) The DFEP $E_0 = (\mathbb{X}^0, \mathbf{0})$ of system (2.4) is globally asymptotically stable if:*

(Z1) *For $\frac{d\mathbb{X}}{dt} = F(\mathbb{X}, 0)$, $\mathbb{X}^0$ is globally asymptotically stable*

(Z2) *$H(\mathbb{X}, \mathbb{Y}) = P\mathbb{Y} - \hat{H}(\mathbb{X}, \mathbb{Y})$ satisfies $\hat{H}(\mathbb{X}, \mathbb{Y}) \geq 0$ in Ω, where:*

- *1. $P = D_{\mathbb{Y}} H(\mathbb{X}^0, 0)$ is Metzler (non-negative off-diagonal elements)*
- *2. Ω is the biologically feasible region*

Theorem 4. *The CoVCom10 model (2.4) is globally asymptotically stable at DFEP E_0 when $R_0 < 1$, satisfying both Castillo-Chavez conditions [24].*

Proof. Firstly, to satisfy condition **(Z1)**, the model (2.4) are rewrite by setting, $T_H = (S, V)$ and, $G_H = (E, U, Q, P, H, C, F, R)$. Then, disease-free equilibrium point is given by the fixed point,

$$\mathbb{E}_0 = \left(\mathbb{X}^0, 0\right) = \left(\frac{\Lambda}{\beta + \mu}, \frac{\beta\,\Lambda}{\mu\,(\beta + \mu)}\right),$$

the system $\frac{dT_H}{dt} = F(T_H, 0)$ becomes,

$$\begin{aligned} \frac{dS^*}{dt} &= \Lambda - (\beta + \mu)\, S, \\ \frac{dV^*}{dt} &= \beta\, S - (\mu)\, V. \end{aligned} \tag{3.37}$$

By solving Eq. (3.37), the equation has a unique equilibrium point,

$$(S^*, V^*) = \left(\frac{\Lambda}{\beta + \mu}, \frac{\beta\,\Lambda}{\mu\,(\beta + \mu)}\right), \tag{3.38}$$

hence $\mathbb{X}^0$ is globally asymptotically stable. So we can say the condition **(Z1)** is fulfilled. Now, to satisfy the second condition **(Z2)**, $H(T_H, G_H) = P_H G_N - \hat{H}(T_H, G_H)$, and

$\hat{H}(T_H, G_H) \geq 0$, For that, system of equations (2.4). We have,

$$H(T_H, G_H) = \begin{bmatrix} E\phi\, S + \gamma\, VE - (\lambda_1 U + \lambda_2 Q + \mu + d_1)\, E \\ \lambda_1 EU - (\alpha_1 + \alpha_2 + \mu + d_2)\, U \\ \lambda_2 EQ - (b_1 + b_2 + b_3 + \mu + d_3)\, Q \\ \alpha_2 U + b_1 Q - (\varphi_1 + \varphi_2 + \varphi_3 + \mu + d_4)\, P \\ \eta\, C + \sigma_2 F + \varphi_1 P - (m_1 + m_2 + m_3 + \mu + d_5)\, H \\ m_2 H + \varphi_2 P - (\eta + \mu + d_6)\, C \\ \varphi_3 F + m_3 H - (\sigma_1 + \sigma_2 + \mu + d_7)\, F \\ \sigma_1 F + m_1 H + \alpha_1 U - (\tau + \mu)\, R \end{bmatrix}, \tag{3.39}$$

$$\hat{H}(T_H, G_H) = P_H G_N - H(T_H, G_H) = \begin{bmatrix} ((\phi(S^* - S) + \gamma(V^* - V) - \lambda_1 U - \lambda_2 Q)E \\ \lambda_1 EU \\ \lambda_2 EQ \\ 0 \\ 0 \\ 0 \\ 0 \\ 0 \end{bmatrix}, \tag{3.40}$$

this shows that, $\hat{H}(T_H, G_H) \geq 0$, where G_N represent an M matrix, it contains a non-negative off-diagonal element. Therefore, Both conditions **(Z1)** and **(Z2)** are satisfied when $R_0 < 1$, proving global asymptotic stability of DFEP E_0 by Lemma 2.

3.3. Existence and Uniqueness of Solution

The mathematical results presented in this section that model (2.4) and (2.5) (CoV-Com10) have a unique solution under certain reasonable assumptions. From an epidemiological viewpoint, the existence of solutions implies that the model reliably predicts disease dynamics, confirming that realistic initial conditions and parameters will always yield a meaningful trajectory of the disease. Uniqueness assures that the models predictions are consistent and reproducible, crucial for decision-making in public health. The CoVCom10 model's solutions, which are provided in system of equation (2.4) and (2.5) are described in this section by their qualitative qualities. The following Volterra-type integral equation results from first taking the both sides integral, where $\int_t^\zeta$ is the integration function having

the order ζ with respect to t Now by using the definition of Khalilzadeh [19, 20], we get,

$$\begin{aligned}
S(t) - S(0) &= \int_0^t \rho^{\zeta-1} \left[\Lambda + \tau R(\rho) + b_2 Q(\rho) - (\phi E(\rho) + \beta + \mu)\, S(\rho)\right] d\rho, \\
E(t) - E(0) &= \int_0^t \rho^{\zeta-1} \left[\phi\, E(\rho) S(\rho) + \gamma\, V(\rho) E(\rho) - (\lambda_1 U(\rho) + \lambda_2 Q(\rho) + \mu + d_1)\, E(\rho)\right] d\rho, \\
U(t) - U(0) &= \int_0^t \rho^{\zeta-1} \left[\lambda_1 E(\rho) U(\rho) - (\alpha_1 + \alpha_2 + \mu + d_2)\, U(\rho)\right] d\rho, \\
Q(t) - Q(0) &= \int_0^t \rho^{\zeta-1} \left[\lambda_2 E(\rho) Q(\rho) - (b_1 + b_2 + b_3 + \mu + d_3)\, Q(\rho)\right] d\rho, \\
P(t) - P(0) &= \int_0^t \rho^{\zeta-1} \left[\alpha_2 I(\rho) + b_1 Q(\rho) - (\varphi_1 + \varphi_2 + \varphi_3 + \mu + d_4)\, P(\rho)\right] d\rho, \\
H(t) - H(0) &= \int_0^t \rho^{\zeta-1} \left[\varphi_1 P(\rho) + \eta\, C(\rho) + \sigma_2 F(\rho) - (m_1 + m_2 + m_3 + \mu + d_5)\, H(\rho)\right] d\rho, \\
C(t) - C(0) &= \int_0^t \rho^{\zeta-1} \left[\varphi_2 P(\rho) + m_2 H(\rho) - (\eta + \mu + d_6)\, C(\rho)\right] d\rho, \\
F(t) - F(0) &= \int_0^t \rho^{\zeta-1} \left[\varphi_3 P(\rho) + m_3 H(\rho) - (\sigma_1 + \sigma_2 + \mu + d_7)\, F(\rho)\right] d\rho, \\
V(t) - V(0) &= \int_0^t \rho^{\zeta-1} \left[\beta\, S(\rho) + b_3 Q(\rho) - (\gamma\, E(\rho) + \mu)\, V(\rho)\right] d\rho, \\
R(t) - R(0) &= \int_0^t \rho^{\zeta-1} \left[\sigma_1 F(\rho) + \alpha_1 I(\rho) + m_1 H(\rho) - (\tau + \mu)\, R(\rho)\right] d\rho,
\end{aligned} \tag{3.41}$$

define the kernels in following,

$$\begin{aligned}
\Phi_1(t, S) &= \Lambda + \tau R(t) + b_2 Q(t) - (\phi E(t) + \beta + \mu)\, S(t), \\
\Phi_2(t, E) &= \phi\, E(t) S(t) + \gamma\, V(t) E(t) - (\lambda_1 U(t) + \lambda_2 Q(t) + \mu + d_1)\, E(t), \\
\Phi_3(t, U) &= \lambda_1 E(t) U(t) - (\alpha_1 + \alpha_2 + \mu + d_2)\, U(t), \\
\Phi_4(t, Q) &= \lambda_2 E(t) Q(t) - (b_1 + b_2 + b_3 + \mu + d_3)\, Q(t), \\
\Phi_5(t, P) &= \alpha_2 U(t) + b_1 Q(t) - (\varphi_1 + \varphi_2 + \varphi_3 + \mu + d_4)\, P(t), \\
\Phi_6(t, H) &= \varphi_1 P(t) + \eta\, C(t) + \sigma_2 F(t) - (m_1 + m_2 + m_3 + \mu + d_5)\, H(t), \\
\Phi_7(t, C) &= \varphi_2 P(t) + m_2 H(t) - (\eta + \mu + d_6)\, C(t), \\
\Phi_8(t, F) &= \varphi_3 P(t) + m_3 H(t) - (\sigma_1 + \sigma_2 + \mu + d_7)\, F(t), \\
\Phi_9(t, V) &= \beta\, S(t) + b_3 Q(t) - (\gamma\, E(t) + \mu)\, V(t), \\
\Phi_{10}(t, R) &= \sigma_1 F(t) + \alpha_1 U(t) + m_1 H(t) - (\tau + \mu)\, R(t)., m
\end{aligned} \tag{3.42}$$

Theorem 5. *(Lipschitz Continuity and Contraction Mapping of Kernel Operators) Let $\Phi_i : \mathbb{R}^+ \times \mathcal{X} \to \mathcal{X}$ $(i = 1, \ldots, 10)$ be kernel operators defined on a Banach space $\mathcal{X}$ with norm $\|\cdot\|$. Assume:*

- *Population compartments are bounded:* $\| S \| \leq r_1$, $\| E \| \leq r_2$, $\| U \| \leq r_3$, $\| Q \| \leq r_4$, $\| P \| \leq r_5$, $\| H \| \leq r_6$, $\| C \| \leq r_7$, $\| F \| \leq r_8$, $\| V \| \leq r_9$, $\| R \| \leq r_{10}$
- *Lipschitz coefficients satisfy:*

$$\begin{aligned} s_1^* &= \phi r_2 + \beta + \mu \\ s_2^* &= \phi r_1 + \gamma r_9 + \Pi_1 \\ s_3^* &= \lambda_1 r_2 + \Pi_2 \\ s_4^* &= \lambda_2 r_2 + \Pi_3 \\ s_5^* &= \Pi_4,\ s_6^* = \Pi_5,\ s_7^* = \Pi_6,\ s_8^* = \Pi_7 \\ s_9^* &= \gamma r_2 + \mu \\ s_{10}^* &= \tau + \mu \end{aligned}$$

- *Parameter constraint:*

$$0 \leq s_i^* < 1 \quad \forall i \in \{1, \ldots, 10\}$$

Then each Φ_i satisfies the Lipschitz condition and constitutes a contraction mapping.

Proof. We demonstrate the result for Φ_1; analogous arguments apply to $\Phi_2, \ldots, \Phi_{10}$. Let $S_1, S_2 \in \mathcal{X}$ be arbitrary functions. Then:

$$\begin{aligned} \| \Phi_1(t, S_1) - \Phi_1(t, S_2) \| =& \| \left[\Lambda + \tau R(t) + b_2 Q(t) - (\phi E(t) + \beta + \mu) S_1(t)\right] \\ & - \left[\Lambda + \tau R(t) + b_2 Q(t) - (\phi E(t) + \beta + \mu) S_2(t)\right] \| \\ =& \| -(\phi E(t) + \beta + \mu)(S_1(t) - S_2(t)) \| \\ \leq& (\phi \| E \| + \beta + \mu) \| S_1 - S_2 \| \quad \text{(by triangle inequality)} \\ \leq& s_1^* \| S_1 - S_2 \|, \end{aligned} \tag{3.43}$$

where $s_1^* = \phi r_2 + \beta + \mu$ by the boundedness assumption $\| E \| \leq r_2$. The contraction property follows from $0 \leq s_1^* < 1$. Similar calculations for $\Phi_2, \ldots, \Phi_{10}$ yield corresponding Lipschitz constants $s_2^*, \ldots, s_{10}^*$ with contraction properties under the stated parameter constraints. Therefore, all kernel operators satisfy both Lipschitz continuity and contraction mapping requirements.

By considering the kernels $\Phi_i,\ i = 1, 2, 3, \ldots, 10$. Now the system of equation have (3.41) then, Recursive formula can be proceed in the following,

$$\mho 1_v = S(t) - S(0) = \int_0^t \rho^{\zeta - 1} \left(\Phi_1(\rho, S_{v-1}) - \Phi_1(\rho, S_{v-2})\right) d\rho, \tag{3.44}$$

triangle inequality law will be apply on Eq. (3.44),

$$\| \mho 1_v \| = \| S_v(t) - S_{v-1}(t) \| \leq s_1^* \int_0^t \rho^{\zeta - 1} \| (S_{v-1} - S_{v-2})) \| d\rho, \tag{3.45}$$

by applying Lipschitz conditions (5),

$$\| \mho 1_v \| \leq s_1^* \int_0^t \| \mho 1_{v-1} \| \, d\rho, \tag{3.46}$$

it can write,

$$S_v(t) = \sum_{i=1}^{v} \mho 1_v(t). \tag{3.47}$$

Similarly for others. Thus the following theorem may be derived from these findings.

Theorem 6. *(Existence of CoVCom10 Model Solutions) Let $\mathcal{X} = C([0, t_{max}], \mathbb{R}^+)$ be the Banach space of continuous functions with norm $\| \cdot \|$. The CoVCom10 model admits a unique solution $(S, E, U, Q, P, H, C, F, V, R) \in \mathcal{X}^{10}$ if:*

- *Lipschitz constants s_i^* from Theorem 1 satisfy:*

$$s_i t_{max} \leq 1. \quad \forall i \in \{1, \ldots, 10\}$$

  where $t_{max} > 0$ is the maximal existence time

- *Initial conditions $(S_0, \ldots, R_0)$ are bounded in $\mathcal{X}$*

Proof. Using the Picard iteration scheme for the integral equations, define successive approximations:

$$S_{v+1}(t) = S_0 + \int_0^t \Phi_1(\rho, S_v(\rho)) d\rho,$$

with analogous definitions for other compartments. From Theorem 1's Lipschitz conditions:

$$\begin{aligned} \| \mho 1_v \| &\leq \| S_0 \| \, (s_1^* t_{\max})^v, \\ &\leq \| S_0 \| \, . (s_1^* t_{\max})^v. \quad \text{(by induction hypothesis)} \end{aligned} \tag{3.48}$$

For residual terms $\beth 1_v(t) := S(t) - S_v(t)$:

$$\begin{aligned} \| \beth 1_v(t) \| &\leq \int_0^t \| \Phi_1(\rho, S) - \Phi_1(\rho, S_{v-1}) \| \, d\rho, \\ &\leq s_1^* \int_0^t \| S - S_{v-1} \| \, d\rho, \\ &\leq (s_1^* t_{\max})^v \| S_0 \| \, . \quad \text{(via recursive estimation)} \end{aligned}$$

Under condition $s_i^* t_{\max} < 1$, we get:

$$\lim_{v \to \infty} \| \beth 1_v(t) \| \leq \lim_{v \to \infty} (s_1^* t_{\max})^v \| S_0 \| = 0.$$

Similar convergence holds for other compartments by identical reasoning. By Banach fixed-point theorem, this establishes existence and uniqueness of solutions in $\mathcal{X}^{10}$.

Theorem 7. *(Uniqueness of Solutions for Fractional CoVCom10 Model) Let $\zeta \in (0,1]$ be the fractional order and $t \in [0,T]$ with $T < \min\{1/s_i^*\}_{i=1}^{10}$. If the kernels Φ_i satisfy:*

- *Lipschitz continuity: $\exists s_i^* > 0$ such that*

$$\| \Phi_i(t,x) - \Phi_i(t,y) \| \leq s_i^* \| x - y \| . \quad \forall x, y \in L^1([0,T])$$

- *Time-domain constraint:*

$$1 - s_i^* t^{\zeta} \geq 0. \quad \forall i \in \{1, \ldots, 10\},\ t \in [0,T]$$

then the fractional CoVCom10 system admits a unique solution $(S, E, U, Q, P, H, C, F, V, R) \in (C[0,T])^{10}$.

Proof. Assume two distinct solutions $\mathbf{X} = (S, \ldots, R)$ and $\mathbf{X}^* = (S^*, \ldots, R^*)$ exist. For the S-compartment:

$$\begin{aligned} \| S(t) - S^*(t) \| &\leq \int_0^t \rho^{\zeta-1} \| \Phi_1(\rho, S) - \Phi_1(\rho, S^*) \| \, d\rho, \\ &\leq s_1^* \int_0^t \rho^{\zeta-1} \| S(\rho) - S^*(\rho) \| \, d\rho. \quad \text{(by Lipschitz condition)} \end{aligned} \tag{3.49}$$

Applying the generalized Gronwall inequality for fractional integrals:

$$\| S(t) - S^*(t) \| \leq \| S_0 - S_0^* \| E_{\zeta}(s_1^* \Gamma(\zeta) t^{\zeta}),$$

where E_ζ is the Mittag-Leffler function. Given identical initial conditions $S_0 = S_0^*$ and $T < (s_1^*)^{-1/\zeta}$, the growth estimate implies:

$$\| S(t) - S^*(t) \| \leq 0 \cdot E_{\zeta}(\cdots) = 0. \quad \forall t \in [0,T]$$

Thus $S(t) \equiv S^*(t)$. Repeating this steps for $E(t), \ldots, R(t)$ using their respective Lipschitz constants $s_2^*, \ldots, s_{10}^*$ completes the proof.

3.4. Optimal Control

To stop COVID-19 from spreading, the effects will be examined by using medicinal treatments. To do this, a set of time-dependent control variables, a_1, a_2, and a_3 have been introduced,

- The implementation of continuous vaccination is represented by a_1,
- The social distancing and lockdown measures is represented by a_2,
- Testing and quarantine strategy is represented by a_3.

The COVID-19 model with proposed optimal control a_1, a_2, and a_3 are part of the following nonautonomous system of nonlinear ordinary differential equations.

$$S' = \Lambda + \tau R + b_2 Q - (\phi E + a_1 + \mu)\, S, \tag{3.50}$$

$$E' = \phi\, ES + \gamma\, VE - (\lambda_1 U + \lambda_2 Q + \mu + d_1)\, E, \tag{3.51}$$

$$U' = \lambda_1 EU - (\alpha_1 + \alpha_2 + \mu + d_2)\, U, \tag{3.52}$$

$$Q' = \lambda_2 EQ - (b_1 + b_2 + b_3 + \mu + d_3)\, Q, \tag{3.53}$$

$$P' = \alpha_2 U + b_1 Q - (\varphi_1 + \varphi_2 + \varphi_3 + \mu + d_4)\, P, \tag{3.54}$$

$$H' = \varphi_1 P + \eta\, C + \sigma_2 F - (a_2 + m_2 + m_3 + \mu + d_5)\, H, \tag{3.55}$$

$$C' = \varphi_2 P + m_2 H - (\eta + \mu + d_6)\, C, \tag{3.56}$$

$$F' = \varphi_3 P + m_3 H - (a_3 + \sigma_2 + \mu + d_7)\, F, \tag{3.57}$$

$$V' = a_1\, S + b_3 Q - (\gamma\, E + \mu + a)\, V, \tag{3.58}$$

$$R' = a_3 F + \alpha_1 U + a_2 H - (\tau + \mu)\, R. \tag{3.59}$$

The discussion of optimal control in the model is done to order to determine the optimum values of a_1,a_2, and a_3 that minimise the objective function $J(a_1(t), a_2(t), a_3(t))$ affected by the differential equations (3.50-3.59). The provided objective function is,

$$\begin{aligned} J(a_1, a_2, a_3) = \min_{a_1, a_2, a_3} \int_0^T [X_1 E + X_2 U + X_3 Q + X_4 P + X_5 F + X_6 C + X_7 H \\ + Y_1 \left(a_1\left(t\right)\right)^2 + Y_2 \left(a_2\left(t\right)\right)^2 + Y_3 \left(a_3\left(t\right)\right)^2] dt. \end{aligned} \tag{3.60}$$

Where T is final time, $X_1, X_2, X_3, X_4, X_5, X_6$, and X_7 are the weight cost of Pre-Symptomatic, Infected, Quarantine, Confirm-positive, Asymptomatic, Hospitalized at intensive care unit and Hospitalized at ordinary ward individuals respectively. Where Y_1, Y_2 and Y_3 are weight costs for each control measurable individuals. In this paper, the weight cost of the optimal control as applied by [25, 26] is measured using a quadratic function that fulfills the optimality criteria. The objective is to identify the optimal control (a_1^*, a_2^*, a_3^*). $J(a_1^*, a_2^*, a_3^*) = \min(a_1, a_2, a_3)$. Where, $(a_1, a_2, a_3) \in \mathbb{U}$, $a_i(t)$ is measurable lebesgue on $[0, T]$, $0 \leq a_i(t) \leq 1,\ i = 1, 2, 3$.

Hamiltonian and Optimality Equation

Pontryangin's Maximum Principle [27] is used to determine the requirements that an optimal control must satisfy. Equations (3.50) and (3.60) are transformed into a problem

of minimising the point-wise Hamiltonian ($\mathbb{H}$) with respect to $a_1(t), a_2(t)$, and $a_3(t)$ as a result of his principle.

$$\begin{aligned}\mathbb{H} &= X_1E + X_2U + X_3Q + X_4P + X_5H + X_6C + X_7F + Y_1\left(a_1\left(t\right)\right)^2 + Y_2\left(a_2\left(t\right)\right)^2 \\ &+ Y_3\left(a_3\left(t\right)\right)^2 + \xi_1[\Lambda + \tau R + b_2Q - (\phi E + a_1 + \mu)\,S] + \xi_2[\phi\, ES + \gamma\, VE - (\lambda_1 U \\ &+ \lambda_2 Q + \mu + d_1)E] + \xi_3[\lambda_1 EU - (\alpha_1 + \alpha_2 + \mu + d_2)\,U] + \xi_4[\lambda_2 EQ - (b_1 + b_2 + b_3 \\ &+ \mu + d_3)Q] + \xi_5[\alpha_2 U + b_1 Q - (\varphi_1 + \varphi_2 + \varphi_3 + \mu + d_4)\,P] + \xi_6[\varphi_1 P + \eta\, C + \sigma_2 F \\ &- (a_2 + m_2 + m_3 + \mu + d_5)\,H] + \xi_7[\varphi_2 P + m_2 H - (\eta + \mu + d_6)\,C] + \xi_8[\varphi_3 P + m_3 H \\ &- (a_3 + \sigma_2 + \mu + d_7)\,F] + \xi_9[a_1\, S + b_3 Q - (\gamma\, E + \mu + a)\,V] + \xi_{10}[a_3 F + \alpha_1 U + a_2 H \\ &- (\tau + \mu)\,R],\end{aligned} \tag{3.61}$$

where (ξ_i), $i = 1, 2, ..., 10$ are adjoint variables associate with $S, E, U, Q, P,\ H, C, F, V$ and, R.

Theorem 8. *For the optimal control (a_2^*, a_2^*, a_3^*) and corresponding state solution $(S, E, U, Q, P, H, C, F, V, R)$ that minimize J over $\mathbb{U}$ of the corresponding system of equation (2.4) having the adjoint variable $\xi_1, ..., \xi_{10}$ such that,*

$$\frac{d\xi_1}{dt} = (\xi_1 - \xi_2)\phi E + (\xi_1 - \xi_9)a_1 - a\xi_1, \tag{3.62}$$

$$\frac{d\xi_2}{dt} = (\xi_1 - \xi_2)\phi S + (\xi_9 - \xi_2)\gamma V + (\xi_2 - \xi_3)\lambda_1 U - (\xi_2 - \xi_4)\lambda_2 Q + \xi_2(\mu + d_1) - X_1, \tag{3.63}$$

$$\frac{d\xi_3}{dt} = (\xi_2 - \xi_3)\lambda_1 E + (\xi_3 - \xi_{10})\alpha_1 + (\xi_3 - \xi_5)\alpha_2 + \xi_3(\mu + d_2) - X_2, \tag{3.64}$$

$$\frac{d\xi_4}{dt} = (\xi_2 - \xi_4)\lambda_2 E + (\xi_4 - \xi_5)b_1 + (\xi_4 - \xi_1)b_2 + (\xi_4 - \xi_9)b_3 + \xi_4(\mu + d_3) - X_3, \tag{3.65}$$

$$\frac{d\xi_5}{dt} = (\xi_5 - \xi_6)\varphi_1 + (\xi_5 - \xi_7)\varphi_2 + (\xi_5 - \xi_8)\varphi_3 + \xi_5(\mu + d_4) - X_4, \tag{3.66}$$

$$\frac{d\xi_6}{dt} = (\xi_6 - \xi_{10})a_2 + (\xi_6 - \xi_7)m_2 + (\xi_6 - \xi_8)m_3 + \xi_6(\mu + d_5) - X_5, \tag{3.67}$$

$$\frac{d\xi_7}{dt} = (\xi_7 - \xi_6)\eta + \xi_7(\mu + d_6) - X_6, \tag{3.68}$$

$$\frac{d\xi_8}{dt} = (\xi_8 - \xi_{10})a_3 + (\xi_8 - \xi_6)\sigma_2 + \xi_8(\mu + d_7) - X_7, \tag{3.69}$$

$$\frac{d\xi_9}{dt} = (\xi_9 - \xi_2)\gamma E + \xi_9(\mu) - \xi_9 a, \tag{3.70}$$

$$\frac{d\xi_{10}}{dt} = \xi_{10}\left(\mu + \tau\right) - \xi_1\tau. \tag{3.71}$$

$\xi_i(T) = 0$, *for* $i = 1, 2, 3....10$ *having conditions,*

$$\begin{gathered}a_1^* = max\{0, min(1, \frac{(\xi_1 - \xi_9)S}{2Y_1})\}, a_2^* = max\{0, min(1, \frac{(\xi_6 - \xi_{10})H}{2Y_2})\}, \\ a_3^* = max\{0, min(1, \frac{(\xi_8 - \xi_{10})F}{2Y_3})\},\end{gathered} \tag{3.72}$$

Proof. Using Pontryagin's maximal principle [28], adjoint system is written as a result of our differentiation of the Hamiltonian with repect to the various states $S, E, U, Q, P, H, C, F, V$ and R.

$$\begin{aligned} &\frac{d\xi_1}{dt} = -\frac{\mathrm{d}\mathbb{H}}{\mathrm{d}S}, \frac{d\xi_2}{dt} = -\frac{\mathrm{d}\mathbb{H}}{\mathrm{d}E}, \frac{d\xi_3}{dt} = -\frac{\mathrm{d}\mathbb{H}}{\mathrm{d}I}, \frac{d\xi_4}{dt} = -\frac{\mathrm{d}\mathbb{H}}{\mathrm{d}Q}, \frac{d\xi_5}{dt} = -\frac{\mathrm{d}\mathbb{H}}{\mathrm{d}P}, \\ &\frac{d\xi_6}{dt} = -\frac{\mathrm{d}\mathbb{H}}{\mathrm{d}H}, \frac{d\xi_7}{dt} = -\frac{\mathrm{d}\mathbb{H}}{\mathrm{d}C}, \frac{d\xi_8}{dt} = -\frac{\mathrm{d}\mathbb{H}}{\mathrm{d}F}, \frac{d\xi_9}{dt} = -\frac{\mathrm{d}\mathbb{H}}{\mathrm{d}V}, \frac{d\xi_{10}}{dt} = -\frac{\mathrm{d}\mathbb{H}}{\mathrm{d}R}. \end{aligned} \tag{3.73}$$

With conditions, $\xi_i(T) = 0$, for $i = 1, 2, 3....10$.
The optimal controls (a_1^*, a_2^*, a_3^*) are characterized by adopting the strategy used by Pontryagin et al., [27], based on the following conditions, $\frac{\partial \mathbb{H}}{\partial a_i}$, for i=1,2,3....10. for a_i^*, the result are,

$$a_1^* = \frac{(\xi_1 - \xi_9)S}{2Y_1}, a_2^* = \frac{(\xi_6 - \xi_{10})H}{2Y_2}, a_3^* = \frac{(\xi_8 - \xi_{10})F}{2Y_3}, \tag{3.74}$$

By including the described control set, initial, and transversal conditions, the optimal control system is generated from the adjoint variable system and the optimal control system.

4. Numerical Results and Discussion

Figure 4 presents a comparison between the model-predicted number of infected individuals (U) and the smoothed daily new COVID-19 cases per 100,000 people reported in the United States from January 2022 onward. The model output is shown in red, while the real-world data is plotted in green. The results demonstrate the alignment of model dynamics with observed trends in case data, highlighting the utility of the proposed compartmental framework for capturing the progression of COVID-19 infections
A numerical simulation of the non-linear integer-order system (2.4) has been performed using the classical fourth-order Runge-Kutta (RK4) method. The initial conditions for all compartments are given by:

$$S(0) = 500, E(0) = 20, U(0) = 10, Q(0) = 8, P(0) = 6, H(0) = 4, F(0) = 2, C(0) = 1, V(0) = 0, R(0) = 0.$$

The system of ordinary differential equations governing the CoVCom10 model was solved using the fourth-order Runge-Kutta (RK4) method, which provides improved accuracy over basic Euler methods through its multi-stage slope calculations. For a general ODE system:

$$\frac{d\mathbf{y}}{dt} = \mathbf{f}(t, \mathbf{y}), \quad \mathbf{y}(t_0) = \mathbf{y}_0$$

where $\mathbf{y} = [S, E, U, Q, P, H, F, C, V, R]^T$, the RK4 method computes each time step as:

$$k_1 = \mathbf{f}(t_n, \mathbf{y}_n)$$

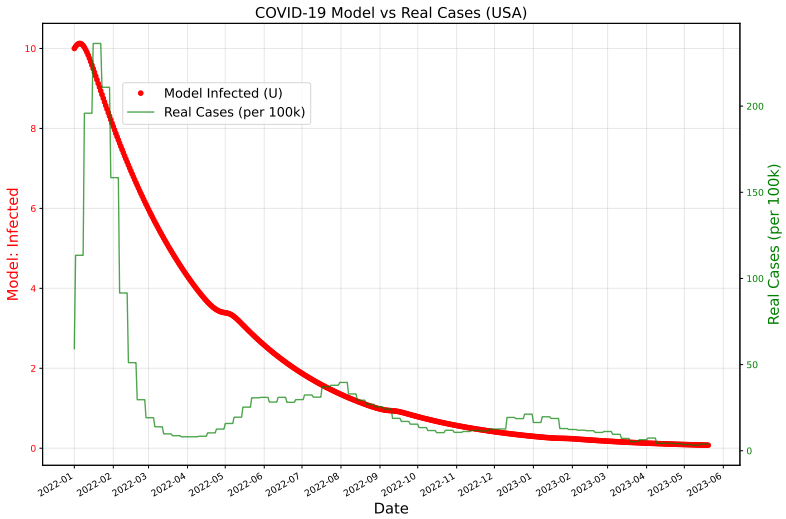

Figure 4: *Comparison of model-predicted infected population (U) with real-world COVID-19 cases per 100,000 people in the United States. The model output is shown in red, and the real-world data is plotted in green.*

$$k_2 = \mathbf{f}\left(t_n + \frac{h}{2}, \mathbf{y}_n + \frac{h}{2}k_1\right)$$
$$k_3 = \mathbf{f}\left(t_n + \frac{h}{2}, \mathbf{y}_n + \frac{h}{2}k_2\right)$$
$$k_4 = \mathbf{f}\left(t_n + h, \mathbf{y}_n + hk_3\right)$$

with the state update given by:

$$\mathbf{y}_{n+1} = \mathbf{y}_n + \frac{h}{6}(k_1 + 2k_2 + 2k_3 + k_4)$$

where h represents the step size controlling temporal resolution. The method's fourth-order accuracy makes it particularly suitable for capturing non-linear epidemiological dynamics while maintaining numerical stability.

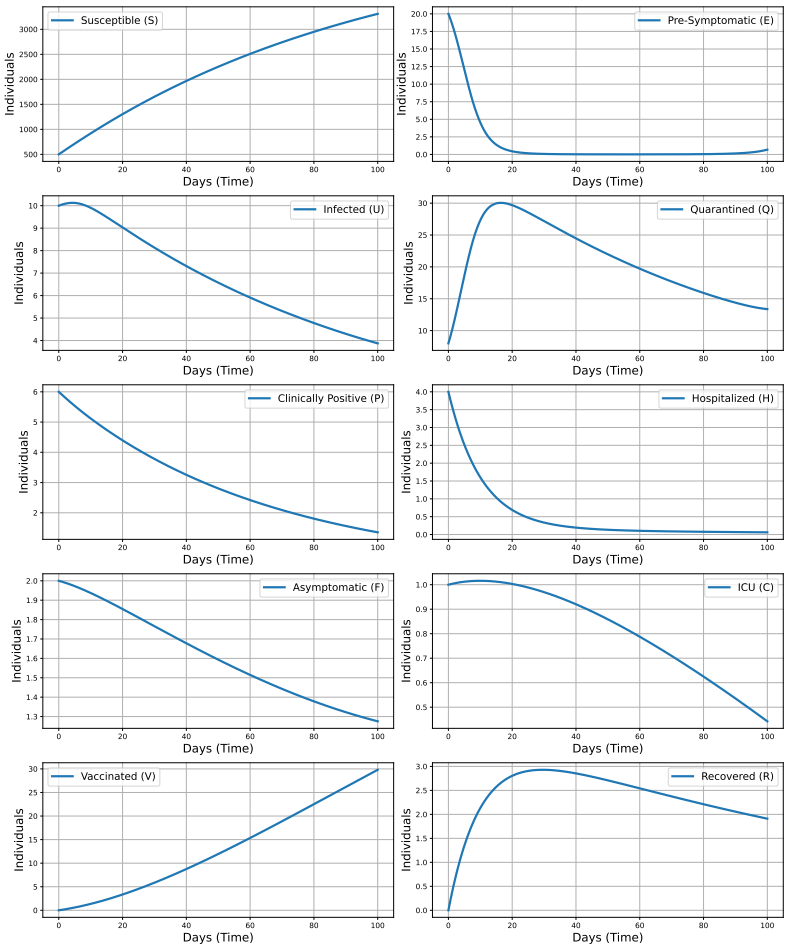

Figure 5: *Time series behavior of COVID-19 model using RK4 method*

The Figure 5 highlight the dynamic evolution of the different compartments in the CoV-Com10 model. The susceptible population increases over time, possibly due to natural recruitment or effective preventive measures reducing disease transmission. The exposed and pre-symptomatic populations decrease, indicating early identification and isolation of cases, which helps prevent further spread. The infected and clinically positive individuals show a gradual decline, suggesting that the disease is being controlled through diagnosis, treatment, and isolation. The quarantined population initially rises and then falls, reflecting efficient identification and management of at-risk individuals. A continuous decrease in hospitalized and ICU cases demonstrates effective healthcare response, while the asymptomatic population also declines, possibly due to detection and reclassification into other compartments. The vaccinated population shows a consistent increase, playing a critical role in protecting susceptible individuals and limiting transmission. The recovered population increases initially and then stabilizes, indicating successful treatment and acquired immunity among the affected individuals. Overall, these results emphasize the impor-

tance of timely public health interventions—such as vaccination, quarantine, treatment, and healthcare support—in curbing the spread of infection and improving population-level health outcomes.

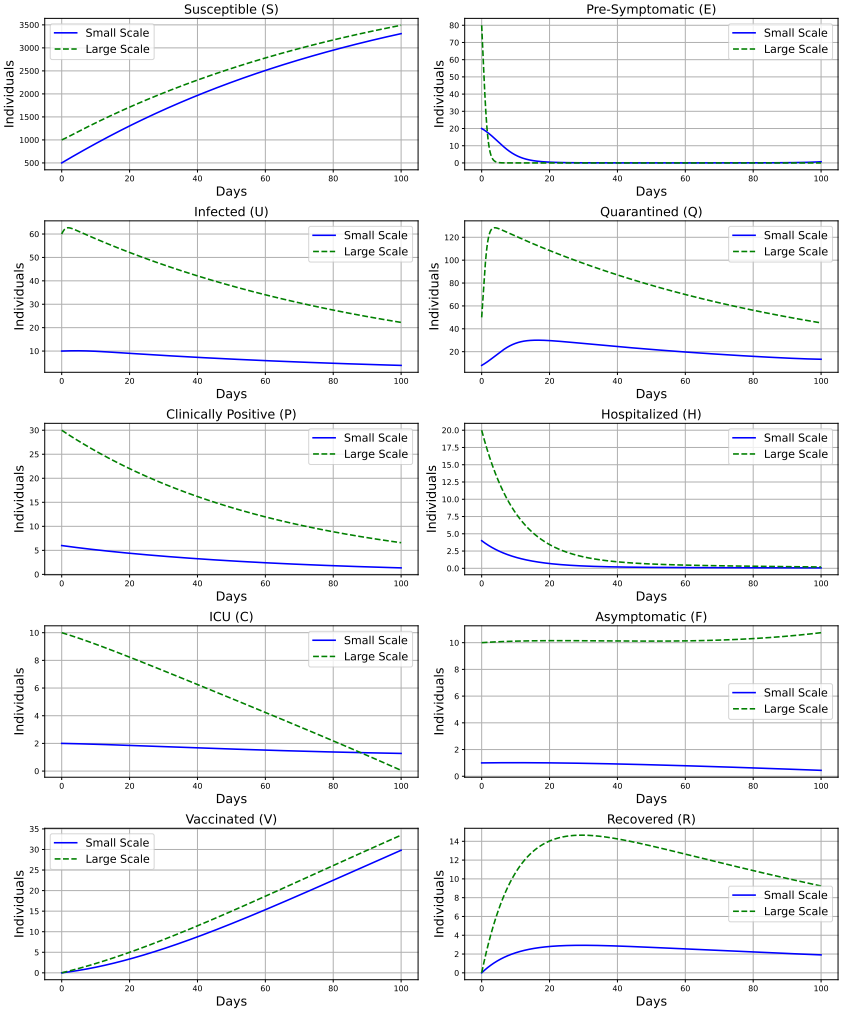

Figure 6: *Comparison of model dynamics under small- and large-scale population settings.*

To evaluate the robustness and reliability of the proposed CoVCom10 model, we conducted simulations using two distinct sets of initial population values. In the *small-scale scenario*, the initial conditions were: $S(0) = 500, E(0) = 20, U(0) = 10, Q(0) = 8, P(0) = 6, H(0) = 4, F(0) = 2, C(0) = 1, V(0) = 0, R(0) = 0$. In contrast, the *large-scale scenario* used proportionally higher values: $S(0) = 1000, E(0) = 80, U(0) = 60, Q(0) = 50, P(0) = 30, H(0) = 20, F(0) = 10, C(0) = 10, V(0) = 0, R(0) = 0$. The comparative outcomes, illustrated in Figure 6, demonstrate that the qualitative behavior of all compartments is consistent across both population scales. While the absolute values increase in line with population size, the temporal progression, peak values, and recovery dynamics remain

largely unchanged. This consistency confirms that the model robustly captures the intrinsic transmission dynamics and is not overly sensitive to variations in initial population sizes.

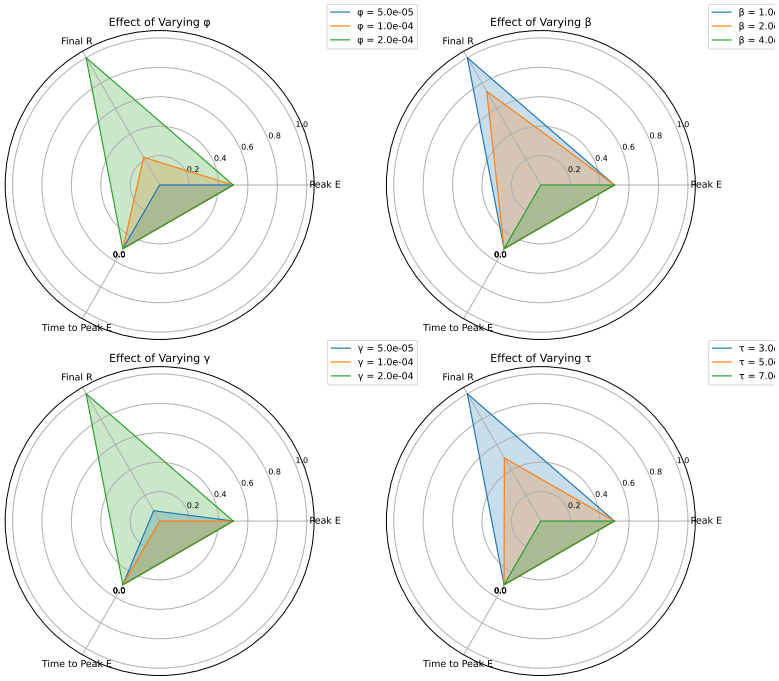

Figure 7: *Radar plots showing the impact of varying ϕ, β, γ, and τ on peak exposed, final recovered, and time to peak exposure.*

Figure 7 presents radar plots illustrating the impact of four parameters ϕ, β, γ, and τ on key epidemic outcomes. Each subplot compares peak exposed (E), final recovered (R), and time to peak E across three values of the selected parameter. Higher ϕ and τ intensify the outbreak by increasing peak E and reducing final R. Conversely, increasing β and γ improves recovery and reduces the epidemic size. Time to peak remains relatively stable under most changes. These results emphasize the role of transmission control and immunity in outbreak management.

4.1. Impact of Optimal Control Strategies on Epidemic Disease Dynamics

This section presents a detailed analysis of the impact of various optimal control strategies on COVID-19 transmission dynamics using the CoVCom10 model. We systematically evaluate the effectiveness of different combinations of interventions, such as vaccination, hospitalization, and management of asymptomatic cases—by applying Pontryagin's Maximum Principle to determine the optimal allocation and timing of these controls. Figure 8 illustrates the temporal evolution of all compartments under scenarios with and without optimal interventions. The simulation results clearly demonstrate that the coordinated implementation of vaccination, enhanced hospitalization capacity, and targeted management

of asymptomatic individuals leads to a substantial reduction in the number of infections and severe cases over time. Notably, the model quantifies the optimal intensity and timing for each control measure, providing actionable guidance for public health authorities to maximize resource efficiency and intervention impact. These findings underscore the critical importance of integrated and sustained public health strategies. By combining multiple interventions, the spread of SARS-CoV-2 can be curbed more effectively and sustainably than by relying on any single measure alone. The numerical results offer practical insights for policymakers, highlighting the value of adaptive, data-driven approaches to epidemic control.

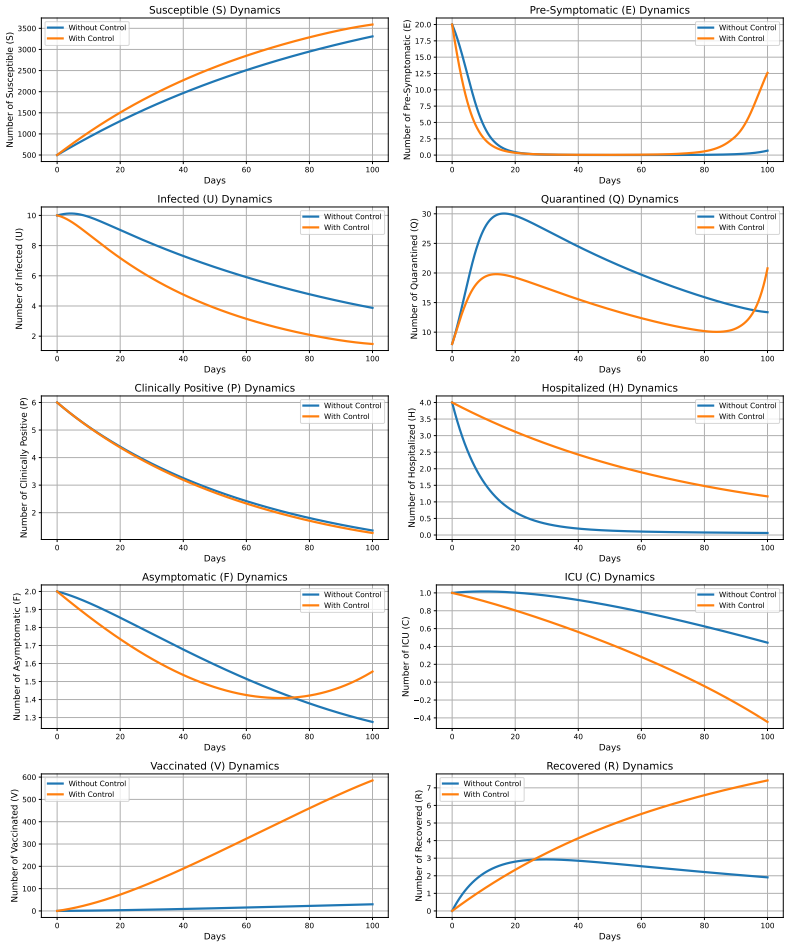

Figure 8: *Temporal dynamics of COVID-19 compartments with and without optimal control interventions.*

4.2. Convergence Analysis of Conformable Fractional Derivative Model

The structural convergence of the conformable fractional system (2.4) was rigorously analyzed through numerical simulations and quantitative error metrics. As demonstrated

in Figure 9, solution trajectories exhibit continuous dependence on the fractional order parameter ς, asymptotically approaching the classical integer-order model (2.1) as $\varsigma \to 1$. The convergence was quantified using the L^2-norm difference:

$$\|\mathbf{y}_\varsigma(t) - \mathbf{y}_1(t)\|_2 = \sqrt{\sum_{i=1}^{10} \int_{t_0}^{t_f} (y_{\varsigma,i}(t) - y_{1,i}(t))^2 dt}$$

where $\mathbf{y}_\varsigma(t) = [S_\varsigma, E_\varsigma, \ldots, R_\varsigma]^T$ and $\mathbf{y}_1(t)$ represent the fractional and integer-order solutions respectively. Numerical solutions were computed using an implicit Runge-Kutta method with adaptive step size control $h \in [0.01, 0.1]$ to maintain relative error tolerance below 10^{-5}.

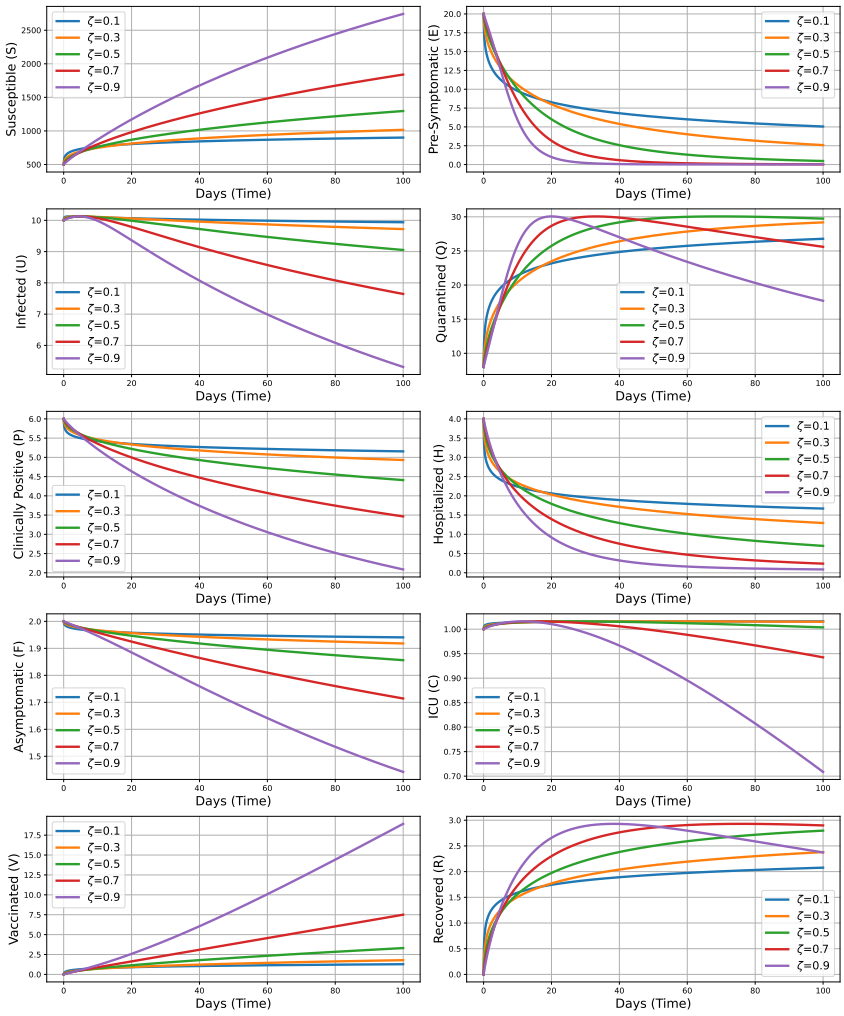

Figure 9: *Dynamic convergence of conformable fractional model solutions to classical solutions as* $\varsigma \to 1$. *Shading represents solution variance across* $\varsigma \in [0.1, 0.9]$.

The conformable fractional derivative introduces time-dependent memory effects into epidemiological modeling, capturing how historical transmission dynamics, immune responses, and behavioral adaptations continuously influence disease spread. Unlike classical integer-order models that assume instantaneous state transitions, the conformable operator $D_t^{\varsigma} y = t^{1-\varsigma} \frac{dy}{dt}$ incorporates a temporal scaling factor $t^{1-\varsigma}$, modulating transmission rates through the fractional order ς. For $\varsigma < 1$, slower infection progression emerges, mimicking real-world delays in interventions such as lockdowns or vaccine rollouts. This formulation avoids non-physical infinite memory artifacts while preserving short-term memory effects, such as waning immunity. By varying $\varsigma \in (0, 1]$, the model spans rapid containment ($\varsigma \to 1$) to prolonged transmission ($\varsigma \ll 1$), reflecting heterogeneous public health scenarios. This approach bridges idealized compartmental frameworks with empirical outbreak patterns, where cumulative interactions dictate epidemic trajectories.

Table 2: *Quantitative convergence analysis of fractional-order solutions*

ς	L^2-Norm Difference	Normalized L^2-Norm
0.1	14986.57	1.0000
0.3	14317.17	0.9553
0.5	12602.19	0.8409
0.7	9295.42	0.6202
0.9	3712.78	0.2477
1.0	0.00	0.0000

Table 3: *Parameters used for the CoVCom10 Model*

Parameters	**Value**	**Source**	**Parameters**	**Value**	**Source**
Λ	50	[12]	λ_1	0.008	[12]
μ	0.009	[12]	λ_2	0.0011	estimated
γ	0.08	estimated	α_1	0.01004	estimated
b_1	0.002	[12]	α_2	0.0083	estimated
b_2	0.0013	estimated	b_3	0.00379	estimated
φ_1	0.001971	[12]	m_1	0.008619	estimated
φ_2	0.0018	estimated	m_2	0.0012	estimated
φ_3	0.004711	[12]	m_3	0.0003	estimated
σ_1	0.0018	estimated	η	0.0009	estimated
σ_2	0.0021	estimated	β	0.5	estimated
β	0.5	[11]	τ	0.05	[11]
ϕ	0.02	estimated	d_1	0.26	[11]
d_2	0.25	estimated	d_5	0.22	estimated
d_3	0.24	estimated	d_6	0.21	estimated
d_4	0.23	estimated	d_7	0.20	estimated

5. Conclusion

This study investigated the impact of vaccination on virus transmission and proposed effective control strategies using a ten-compartment mathematical model named CoV-Com10, formulated as a system of nonlinear differential equations. The model explicitly includes vaccination, asymptomatic, and pre-symptomatic carriers to better capture the real-world transmission dynamics. Our results highlight the critical role of vaccination in mitigating SARS-CoV-2 spread. The model alters the classical susceptible population expression from $S_0 = \frac{\Lambda}{\mu}$ (as seen in SEIR models) to $S_0 = \frac{\Lambda}{\beta+\mu}$ in CoVCom10, reflecting immunization's role in reducing susceptibility. The basic reproduction number R_0 was computed to quantify disease potential. Stability analysis confirms that the disease-free equilibrium is locally and globally asymptotically stable when $R_0 < 1$, and the endemic equilibrium is stable when $R_0 > 1$. Time-dependent control variables for vaccination (a_1), hospitalization (a_2), and asymptomatic isolation (a_3) were introduced via the Pontryagin Maximum Principle. Simulations demonstrated that optimizing these controls significantly reduces transmission. Model parameters such as ϕ, β, and γ reflect real-world biological mechanisms of infection, recovery, and exposure. The success of these strategies depends on coordinated policy implementation and community behavior. Moreover, the modularity of CoVCom10 makes it adaptable to other infectious diseases like influenza or monkeypox, or emerging SARS-CoV-2 variants. Adjusting compartments and parameters allows the model to simulate various epidemiological scenarios. The use of the conformable fractional derivative enhances the model's ability to capture memory effects and persistent behavior. We recommend that vaccination campaigns be complemented by personal preventive practices such as mask-wearing, hand hygiene, and social distancing. These combined interventions are essential for managing current and future infectious disease outbreaks. As a limitation of the model, despite its validation against real epidemiological data, it assumes homogeneous mixing and does not account for spatial heterogeneity or stochastic variations. Additionally, due to limited data availability, some parameters were estimated, which may affect the model's precision. Future work could enhance this model by incorporating stochastic processes, spatial heterogeneity, with co-infection or network-based transmission to provide more realistic and robust policy guidance.

Acknowledgements

Authors (Dr. Nadeem Abbas and Prof. Dr. Wasfi Shatanawi) would like to thank Prince Sultan University for their support through the TAS research lab.

Data Availability
No data availability

Conflict of Interest
The authors declare that there is no conflict of interest.

References

[1] Qun Li, Xuhua Guan, Peng Wu, Xiaoye Wang, Lei Zhou, Yeqing Tong, Ruiqi Ren, Kathy SM Leung, Eric HY Lau, Jessica Y Wong, et al. Early transmission dynamics in wuhan, china, of novel coronavirus–infected pneumonia. *New England journal of medicine*, 382(13):1199–1207, 2020.

[2] Sk Shahid Nadim and Joydev Chattopadhyay. Occurrence of backward bifurcation and prediction of disease transmission with imperfect lockdown: A case study on covid-19. *Chaos, Solitons & Fractals*, 140:110163, 2020.

[3] Joseph T Wu, Kathy Leung, and Gabriel M Leung. Nowcasting and forecasting the potential domestic and international spread of the 2019-ncov outbreak originating in wuhan, china: a modelling study. *The lancet*, 395(10225):689–697, 2020.

[4] Sansao A Pedro, Frank T Ndjomatchoua, Peter Jentsch, Jean M Tchuenche, Madhur Anand, and Chris T Bauch. Conditions for a second wave of covid-19 due to interactions between disease dynamics and social processes. *Frontiers in Physics*, 8:574514, 2020.

[5] Li-Xiang Feng, Shuang-Lin Jing, Shi-Ke Hu, De-Fen Wang, Hai-Feng Huo, et al. Modelling the effects of media coverage and quarantine on the covid-19 infections in the uk. *Math. Biosci. Eng*, 17(4):3618–3636, 2020.

[6] Muhammad Riaz, Kamal Shah, Thabet Abdeljawad, Inas Amacha, Asma Al-Jaser, and Manar Alqudah. A comprehensive analysis of covid-19 nonlinear mathematical model by incorporating the environment and social distancing. *Scientific Reports*, 14(1):12238, 2024.

[7] Eyup Cetin, Serap Kiremitci, and Baris Kiremitci. Developing optimal policies to fight pandemics and covid-19 combat in the united states. *European Journal of Pure and Applied Mathematics*, 13(2):369–389, 2020.

[8] Yasir Nawaz, Muhammad Shoaib Arif, and Kamaleldin Abodayeh. Predictor–corrector scheme for electrical magnetohydrodynamic (mhd) casson nanofluid flow: a computational study. *Applied Sciences*, 13(2):1209, 2023.

[9] Yasir Nawaz, Muhammad Shoaib Arif, Kamaleldin Abodayeh, Muhammad Usman Ashraf, and Mehvish Naz. A new explicit numerical scheme for enhancement of heat transfer in sakiadis flow of micro polar fluid using electric field. *Heliyon*, 9(10), 2023.

[10] Muhammad Farhan, Zahir Shah, Rashid Jan, and Saeed Islam. A fractional modeling approach of buruli ulcer in possum mammals. *Physica Scripta*, 98(6):065219, 2023.

[11] ML Diagne, H Rwezaura, SY Tchoumi, and JM Tchuenche. A mathematical model of covid-19 with vaccination and treatment. *Computational and Mathematical Methods in Medicine*, 2021(1):1250129, 2021.

[12] Edward Acheampong, Eric Okyere, Samuel Iddi, Joseph HK Bonney, Joshua Kiddy K Asamoah, Jonathan AD Wattis, and Rachel L Gomes. Mathematical modelling of earlier stages of covid-19 transmission dynamics in ghana. *Results in Physics*, 34:105193, 2022.

[13] AIK Butt, W Ahmad, M Rafiq, N Ahmad, and M Imran. Optimally analyzed fractional coronavirus model with atangana–baleanu derivative. *Results in Physics*,

53:106929, 2023.

[14] Syeda Alishwa Zanib, Tamour Zubair, Sehrish Ramzan, Muhammad Bilal Riaz, Muhammad Imran Asjad, and Taseer Muhammad. A conformable fractional finite difference method for modified mathematical modeling of sar-cov-2 (covid-19) disease. *PloS one*, 19(10):e0307707, 2024.

[15] Azhar Iqbal Kashif Butt, Waheed Ahmad, Hafiz Ghulam Rabbani, Muhammad Rafiq, Shehbaz Ahmad, Naeed Ahmad, and Saira Malik. Exploring optimal control strategies in a nonlinear fractional bi-susceptible model for covid-19 dynamics using atangana-baleanu derivative. *Scientific Reports*, 14(1):31617, 2024.

[16] Hamadjam Abboubakar and Reinhard Racke. Mathematical modeling of the coronavirus (covid-19) transmission dynamics using classical and fractional derivatives. 2022.

[17] Komal Sharma, Vivek Srivastava, and Ravi Kant Singh. From data to cures: leveraging machine learning, deep learning and pharmacore modelling for targeted therapies. In *AIP Conference Proceedings*, volume 3254, page 020008. AIP Publishing LLC, 2025.

[18] Our World in Data. Covid-19 dataset. https://covid.ourworldindata.org/data/owid-covid-data.csv.

[19] Roshdi Khalil, Mohammed Al Horani, Abdelrahman Yousef, and Mohammad Sababheh. A new definition of fractional derivative. *Journal of computational and applied mathematics*, 264:65–70, 2014.

[20] Nadeem Abbas, Syeda Alishwa Zanib, Sehrish Ramzan, Aqsa Nazir, and Wasfi Shatanawi. A conformable mathematical model of ebola virus disease and its stability analysis. *Heliyon*, 10(16), 2024.

[21] Pauline Van den Driessche and James Watmough. Reproduction numbers and subthreshold endemic equilibria for compartmental models of disease transmission. *Mathematical biosciences*, 180(1-2):29–48, 2002.

[22] Helena Sofia Rodrigues, M Teresa T Monteiro, and Delfim FM Torres. Seasonality effects on dengue: basic reproduction number, sensitivity analysis and optimal control. *Mathematical Methods in the Applied Sciences*, 39(16):4671–4679, 2016.

[23] SM Ashrafur Rahman. *Study of infectious diseases by mathematical models: predictions and controls*. 2016.

[24] Carlos Castillo-Chavez, Sally Blower, Pauline van den Driessche, Denise Kirschner, and Abdul-Aziz Yakubu. *Mathematical approaches for emerging and reemerging infectious diseases: models, methods, and theory*, volume 126. Springer Science & Business Media, 2002.

[25] Getachew Teshome Tilahun, Oluwole Daniel Makinde, and David Malonza. Modelling and optimal control of typhoid fever disease with cost-effective strategies. *Computational and mathematical methods in medicine*, 2017(1):2324518, 2017.

[26] Getachew Teshome Tilahun, Oluwole Daniel Makinde, and David Malonza. Co-dynamics of pneumonia and typhoid fever diseases with cost effective optimal control analysis. *Applied Mathematics and Computation*, 316:438–459, 2018.

[27] Lev Semenovich Pontryagin. *Mathematical theory of optimal processes*. Routledge,

2018.

[28] K Renee Fister, Suzanne Lenhart, and Joseph Scott McNally. Optimizing chemotherapy in an hiv model. 1998.